

**EXPLAINING AND FORECASTING INTERANNUAL VARIABILITY IN  
THE FLOW OF THE NILE RIVER**

Mohamed S. Siam<sup>1</sup>

Ralph M. Parsons Laboratory, Massachusetts Institute of Technology, Cambridge,  
Massachusetts

Elfatih A. B. Eltahir

Ralph M. Parsons Laboratory, Massachusetts Institute of Technology, Cambridge,  
Massachusetts

---

<sup>1</sup>*Corresponding author address:* Mohamed Siam, Ralph M. Parsons Laboratory, Massachusetts  
Institute of Technology, 15 Vassar St. Cambridge, MA 02139.  
E-mail:msiam@mit.edu

1     **EXPLAINING AND FORECASTING INTERANNUAL VARIABILITY IN**  
2                     **THE FLOW OF THE NILE RIVER**

3  
4                     **Abstract**

5  
6     This study analyzes extensive data sets collected during the 20<sup>th</sup> century and define four modes of  
7     natural variability in the flow of Nile River, identifying a new significant potential for improving  
8     predictability of floods and droughts. Previous studies have identified a significant teleconnection  
9     between the Nile flow and the Eastern Pacific Ocean. El Niño-Southern Oscillation (ENSO)  
10    explains about 25% of the interannual variability in the Nile flow. Here, this study identifies a  
11    region in the southern Indian Ocean with similarly strong teleconnection to the Nile flow. Sea  
12    Surface Temperature (SST) in the region (50°E-80°E and 25°S-35°S) explains 28% of the  
13    interannual variability in the Nile flow. During those years with anomalous SST conditions in both  
14    Oceans, this study estimates that indices of the SSTs in the Pacific and Indian Oceans can  
15    collectively explain up to 84% of the interannual variability in the flow of Nile. Building on these  
16    findings, this study uses classical Bayesian theorem to develop a new hybrid forecasting algorithm  
17    that predicts the Nile flow based on global models predictions of indices of the SST in the Eastern  
18    Pacific and Southern Indian Oceans.

21 **1. Introduction**

22 The Nile basin covers an area of  $2.9 \times 10^6$  km<sup>2</sup>, which is approximately 10% of the African  
23 continent (Fig. 1). It has two main tributaries; the White Nile and the Blue Nile that originate from  
24 the equatorial lakes and Ethiopian highlands respectively. The Upper Blue Nile (UBN) basin is  
25 the main source of water for the Nile River. It contributes to approximately 60% of the annual flow  
26 of the Nile and 80% of the total Nile flow that occurs between July and October at Dongola  
27 (Conway and Hulme, 1993) (Fig. 2). The UBN basin extends over an area of  $175 \times 10^3$  km<sup>2</sup> (7° N  
28 to 12°5' N and from 34°5' E to 40° E). The mean annual rainfall over this basin is 1200 mm/year  
29 (Conway and Hulme, 1993). Almost 60% of the annual rainfall over the UBN occurs during the  
30 summer between July and August, resulting in a largely predictable seasonal variability in the flow  
31 of the river.

32

33 The predictability of inter-annual variability in the flow of the Nile is rather challenging. Many  
34 studies investigated the teleconnections between the Ethiopian rainfall and the global SSTs in order  
35 to find SSTs indices to use for Nile flow prediction (e.g. Eltahir, 1996; Abteu et al., 2009; and  
36 Melesse et al., 2011). Eltahir, 1996 showed that the SSTs anomalies over the tropical Eastern  
37 Pacific Ocean explains 25% of the inter-annual variability of Nile flow. ElSanabary et al., 2014  
38 showed that the dominant frequencies of the Ethiopian rainfall ranged between 2 and 8 years and  
39 that the scale averaged wavelet power of the SSTs over the Eastern Pacific and South Indian and  
40 Atlantic Oceans can explain significant fraction of the rainfall variability over Ethiopia using  
41 wavelet principal component analysis. These correlations were the basis for new forecast models  
42 that were proposed to predict the Nile flows. For example, Wang and Eltahir (1999) used a  
43 discriminant prediction approach to estimate the probabilities that the Nile flow will fall into

44 prescribed categories. Eldaw et al., (2003) and Gissila et al., (2004) used sea surface temperature  
45 (SST) over the Pacific, Indian and Atlantic Oceans as predictors within a multiple linear regression  
46 model to predict the Nile flow.

47

48 The mechanisms behind these teleconnections between the rainfall over Ethiopia and the global  
49 SSTs were examined in several studies (e.g. Beltrando and Camperlin, 1993). However, a clear  
50 distinction must be made between rainfall over the UBN basin in Ethiopia and rainfall over East  
51 Africa, defined as the region along the coast, east of the Ethiopian highlands (Fig. 1). The UBN  
52 basin has one rainy season (May to September) during which more than 80% of the rainfall occurs,  
53 while along the East coast of Africa and depending on the location from the equator, the seasonal  
54 cycle of rainfall can have two rainy seasons (Black et al., 2003, Hastenrath et al., 2011). This  
55 pattern in the seasonal cycle of rainfall is related to the migration of the Inter-tropical Convergence  
56 Zone (ITCZ) across the equator. Camberlin, 1995 showed that the rainfall over East Africa,  
57 including the UBN basin, is strongly coupled with the dynamics of the Indian monsoon. During  
58 strong Indian monsoon seasons, the sea level pressure over India decreases significantly, which  
59 enhances the pressure gradient between East Africa and India. As a result, westerly winds increase  
60 over Eastern Africa, which advect moisture from the Congo basin to Ethiopia, Uganda and western  
61 Kenya. Giro et al., 2010 also showed that the warming over the Pacific Ocean, during El Niño  
62 events, reduces these westerly winds, which reduce the rainfall over East Africa. In addition, the  
63 monsoon circulation is weaker during El Niño events due to modulation of the walker circulation  
64 and enhanced subsidence over the Western Pacific and South Asia, thus the rainfall over Ethiopia  
65 decreases (Ju and Slingo, 1995; Kawamura, 1998; Shukla and Wallace, 1983; Soman and Slingo,  
66 1997). The reduced Nile flows during El Niño events were also attributed to the enhanced tropical-

67 scale subsidence that suppresses rainfall, as a consequence of the increased upwelling over the  
68 Eastern Pacific Ocean (Amarasekera et al., 1996).

69  
70 The teleconnection between the Nile flow and SSTs of North and Middle Indian Ocean and ENSO  
71 is described in another paper by the authors (Siam et al., 2014). Nile flow is strongly modulated  
72 by ENSO through ocean currents. During El Niño events, the warm water travels from the Pacific  
73 to the Indian Ocean through the “Indonesian through flow” and advection by the Indian Equatorial  
74 Current (Tomczak and Godfrey, 1995). As a result, SSTs in North and Middle Indian Ocean warm-  
75 up following the warming of Tropical Eastern Pacific, and forces a Gill type circulation anomaly  
76 with enhanced westerly winds over Western Indian Ocean (Yang et al., 2007). The latter enhances  
77 the low-level divergence of air and moisture away from the Upper Blue Nile resulting in a  
78 reduction of rainfall over the basin. On the other hand, the warming over the South Indian Ocean,  
79 generates a cyclonic flow in the boundary layer, which reduces the cross-equatorial meridional  
80 transport of air and moisture towards the UBN basin, favoring a reduction in rainfall and river  
81 flows. The tele-connections between the Pacific Ocean and the Nile basin and between the Indian  
82 Ocean and the Nile basin are reflected in different modes of observed natural variability in the  
83 flow of Nile River, with important implications for the predictability of floods and droughts.

84  
85 The objectives of the study are (i) to investigate the teleconnection between the Indian Ocean and  
86 the Nile basin and its role in explaining observed natural modes of variability in the flow of the  
87 Nile river, and (ii) to develop a new hybrid forecasting algorithm that can be used to predict the  
88 Nile flow based on indices of the SST in the Eastern Pacific and Southern Indian Oceans.

89

## 90 **2. Data**

91 In this study we use observed SSTs over the Indian and Pacific oceans from the monthly global  
92 (HadISST V1.1) dataset on a 1 degree latitude-longitude grid from 1900 to 2000 (Rayner et al.  
93 2003). The monthly flows at Dongola from 1900 to 2000 were extracted from the Global River  
94 Discharge Database (RivDIS v1.1) (Vörösmarty et al., 1998). The average monthly anomalies  
95 from September to November of the SSTs averaged over the Eastern Pacific Ocean (6°N-2°N,  
96 170°W-90°W; 2°N-6°S, 180°W-90°W; and 6°S-10°S, 150°W-110°W) are used as an index of  
97 ENSO. This area has shown the highest correlation with the Nile flows and it is almost covering  
98 the same area as Niño 3 and 3.4 indices (Trenberth, 1997).

99

## 100 **3. Relation between the variability in the flow of Nile river, ENSO and the Indian Ocean SST**

101 Based on extensive correlation analysis of the Nile river flow at Dongola and the observed SST in  
102 the Indian Ocean, this study identifies a region over the Southern Indian Ocean (50°E-80°E and  
103 25°S-35°S) (see Figure 3) as the one with the highest correlation between SST and the Nile flow.  
104 This correlation is especially high for river flow (accumulated for July, August, September and  
105 October) and SST during the month of August. In comparison to earlier studies, ElDaw et al.  
106 (2003) used SST indices over the Indian Ocean to predict the Nile flow, however, they focused on  
107 regions of the Indian Ocean that are different from the region that we use in defining the SIO index.  
108 In other words the region of the SIO was not used by ElDaw et al. (2003). Table 2 describes the  
109 regions of the Indian Ocean identified in both studies.

110

111 Here, this study emphasizes that the proposed forecasting methodology for the Nile flow is  
112 motivated by the physical mechanisms proposed by Siam et al. (2014) and described in Section 1.

113 However, the forecasting approach of some of the previous studies was based on purely statistical  
114 correlations found between the Nile flow and SSTs globally.

115  
116 Figure 4 shows the observed and simulated time series of the average July to October Nile flow at  
117 Dongola, which accounts for approximately 70% of the annual Nile flow. The Nile flow is  
118 predicted by a linear regression model using ENSO averaged from September to November and  
119 SIO August indices as predictors. It is clear from this figure that the addition of the SIO index  
120 increase the explained variability of the Nile flow to 44%, compared to only 25% when ENSO  
121 index is used alone. This indicates that the SIO index can explain almost 20% of the variability of  
122 the Nile flow that is independent from ENSO. The North and middle of the Indian Ocean have  
123 also exhibited a high correlation between their SST and the Nile flow. However, the additional  
124 variability explained by the SST over the North and Middle Indian Ocean, when combined with  
125 the ENSO index, is negligible (not shown here). This is mainly because the SSTs over the North  
126 and Middle Indian Ocean are dependent on ENSO, while the SSTs over the South Indian Ocean  
127 (i.e. SIO index) is not, as described in Section 1.

128  
129 In further analysis, we define  $\pm 0.5^{\circ}\text{C}$  as the threshold between non-neutral and neutral years on the  
130 Eastern Pacific Ocean based on ENSO index. This value is about two-thirds of one standard  
131 deviation of the anomalies of ENSO index. The same threshold has been used to identify non-  
132 neutral and neutral years using El Niño 3.4 index, which is similar to our ENSO index (Trenberth,  
133 1997). This indicates that if the ENSO index anomaly is greater than  $0.5^{\circ}\text{C}$  or less than  $-0.5^{\circ}\text{C}$ , it  
134 is considered as non-neutral condition, otherwise, it is considered as neutral condition. Similarly,

135  $\pm 0.3^{\circ}\text{C}$  value is used as a threshold between non-neutral and neutral years on the South Indian  
136 Ocean using the SIO index. This value is also about two-thirds of one standard deviation for the  
137 anomalies of the SSTs over this region. Thus, if both ENSO and SIO indices are used together,  
138 four different combinations can be defined based on these classifications. The first is when both  
139 ENSO and SIO indices are neutral (29 out of 100 events), the second is when both ENSO and SIO  
140 indices are non-neutral (19 out of 100 events), the third when SIO is non-neutral and ENSO is  
141 neutral (26 out of 100 events) and finally when SIO is neutral and ENSO is non-neutral (26 out of  
142 100 events). Each of these combinations is considered as a mode of natural variability in the flow  
143 of Nile river. Then the Nile flow is calculated as a predictant using multiple linear regression with  
144 the (ENSO and SIO indices) of each mode as predictors.

145

146 Four different modes are identified for describing the natural variability in the flow of Nile River  
147 and summarized in (Table 1). The ENSO and SIO indices do not explain a significant fraction of  
148 the interannual variability in the flow of river when they are both neutral (Fig. 5a). The variability  
149 of the Nile flow in such years can be regarded as a reflection of the chaotic interactions between  
150 the biosphere and atmosphere and within each of the two domains. For this mode, the predictability  
151 of the Nile flow is rather limited. The other two intermediate modes include non-neutral conditions  
152 in the Eastern Pacific and neutral conditions in the Southern Indian Oceans or vice versa (Fig. 5b  
153 and 5c). For these two modes, a significant fraction (i.e. 31% and 43%) of the variance describing  
154 inter-annual variability in the flow is explained. Hence, these modes point to a significant potential  
155 for predictability of the flow. Finally, indices of ENSO and SIO can explain 84% of the interannual  
156 variability in the Nile flow when non-neutral conditions are observed for both the Eastern Pacific  
157 and Southern Indian Oceans (Fig. 5d). Therefore, the SIO index can be used to predict the flow



158 together with the ENSO index, as collectively they can explain a significant fraction of the  
159 variability in the flow of Nile River. This result indicates that during years with anomalous SST  
160 conditions in both oceans, floods and droughts in the Nile River flow can be highly predictable,  
161 assuming accurate forecasts of those indices are available.

162

#### 163 **4. A Hybrid Methodology for Long-range Prediction of the Nile flow**

164 A simple methodology is proposed to predict the Nile flow with a lead time of about a few months  
165 (~3-6 months). The forecast of global SST distribution based on dynamical models (e.g. NCEP  
166 coupled forecast system model version 2 (CFSv2), Saha et al., 2010; Saha et al., under review),  
167 can be used together with the algorithm developed in this section to relate the Nile flow to ENSO  
168 and SIO indices. The proposed method is shown in Figure 6 and can be described in two main  
169 steps:

- 170 • Forecast of SST anomalies in the Indian Ocean and Eastern Pacific Ocean using dynamical  
171 models of the coupled global ocean atmosphere system. Such forecasts are routinely issued by  
172 centers such NCEP and ECMWF.
- 173 • Application of a forecast algorithm between the Nile flow (predictand) and forecasted SSTs  
174 in the Indian and Eastern Pacific Oceans (predictors) for the identified mode of variability.

175

176 In this paper we focus on the second step of the proposed method: the development of the algorithm  
177 relating SSTs and the Nile flow. We develop the forecast algorithm using observed SSTs. We do  
178 not describe how this algorithm can be applied with forecasts of global SST distribution based on

179 dynamical models as this step is beyond the scope of this paper. However, we recognize that  
180 overall accuracy of this method in predicting interannual variability of the Nile flow is dependent  
181 on the skill of global coupled models in forecasting the global SSTs (See Appendix for information  
182 about forecasting models). Thus, the selection of the forecast model, which predicts the SSTs is  
183 an important step to ensure the accuracy of the prediction of the Nile flow. As global coupled  
184 ocean-atmosphere models improve in their skill of forecasting global SSTs in the Pacific and  
185 Indian Oceans, we expect that our ability to predict the interannual variability in the Nile flow will  
186 improve too. In addition, the accuracy in the prediction of the Nile flow at medium and short time  
187 scales (of weeks to one month) can be improved by adding other hydrological variables (e.g.  
188 rainfall and stream flow) over the basin, as demonstrated by (Wang and Eltahir, 1999)

189 The proposed method can be described as hybrid since it combines dynamical forecasts of global  
190 SSTs, and statistical algorithms relating the Nile flow and the forecasted SSTs. The same method  
191 can also be described as hybrid since it combines information about SSTs from the Pacific and the  
192 Indian Oceans.

193 Here, we apply a discriminant approach that specifies the categoric probabilities of the predictand  
194 (Nile flow) according to the categories that the predictors (i.e. ENSO and SIO indices) fall into.  
195 The annual Nile flow is divided into “low”, “normal”, and “high” categories. The boundaries of  
196 these categories are defined so that the number of points in each category is about a third of the  
197 data points (Fig 7). On the other hand, the ENSO and SIO indices are divided into “cold”, “normal”  
198 and “warm” categories. (The words Normal and Neutral are used to describe the same  
199 conditions).The boundaries for the normal category are  $-0.5^{\circ}\text{C}$  and  $0.5^{\circ}\text{C}$  for ENSO index and -  
200  $0.3^{\circ}\text{C}$  and  $0.3^{\circ}\text{C}$  for SIO index (Fig. 7). Any condition below the lower limit is considered “cold”  
201 and higher than the upper limit is considered “warm” for both indices.

202 The Bayesian theorem, described in many statistical books (e.g., Winkler 1972; West 1989), states  
 203 that the probability of occurrence of a specified flow category ( $Q_i$ ) and given two conditions (A  
 204 and B) can be expressed as

$$205 \quad P(Q_i / A, B) = \frac{P(B/Q_i, A)P(Q_i/A)}{P(B/A)} \quad (1)$$

206 Where  $P(Q_i / A)$  is the probability of event  $Q_i$  given that event A has occurred, and  $P(Q_i / A, B)$  is  
 207 the probability of event  $Q_i$  given that events A and B have occurred, and similarly for other shown  
 208 probabilities. In addition, if the events A and B are independent, we can rewrite Eq. (1) as

$$209 \quad P(Q_i / A, B) = \frac{P(B/Q_i)P(Q_i/A)}{\sum_{i=1}^3 P(B/Q_i)P(Q_i/A)} \quad (2)$$

210 The advantage of assuming independence between (A and B) and using Eq. (2), it simplifies the  
 211 calculation of  $P(B/Q_i, A)$  since we do not have to split the data into a relatively large number of  
 212 categories, which reduces the error due to the limitation of the data size. The independence  
 213 between ENSO and SIO indices is a reasonable assumption as the coefficient of determination  
 214 between them is less than 6%.

215

216 In order to evaluate the predictions of the Nile flow, we use a forecasting index (FI) defined by  
 217 Wang and Eltahir, (1999) as

$$218 \quad FP(j) = \sum_{i=1}^3 P_r(i, j) P_p(i, j) \quad (3)$$

$$219 \quad FI = \frac{1}{n} \sum_{i=1}^n FP(j) \quad (4)$$

220 Where  $FP(j)$  is the forecast probability in a certain year ( $j$ ) and the FI is the average of the FP over  
221 a certain period,  $n$ . The prior probability  $P_r(i, j)$  is calculated using Eq.(2) for a certain year ( $j$ ) and  
222 category ( $i=1, 2, 3$ ) and the posterior probability  $P_p(i, j)$  is defined as  $[1,0,0]$  in low flow year,  
223  $[0,1,0]$  in normal year, and  $[0,0,1]$  in a high flow year. Hence, a larger FI indicates a higher  
224 accuracy of the forecast. The FI without any information about SST, should be about one third as  
225 we have classified flow data into three categories each with a similar number of the data points.

226 The data is split into a calibration period (1900-1970) and a verification period (1970-2000).  
227 Tables 3 and 4 summarize the conditional probabilities of Nile flow given certain conditions of  
228 SIO or ENSO index. It is shown that during “warm” and “cold” conditions of SIO, the probabilities  
229 are significantly higher for “low” and “high” Nile flow, respectively. The same is true for the  
230 ENSO, as was described originally by Eltahir (1996). Table 5 shows the probabilities that are  
231 conditioned on both SIO and ENSO, calculated using Eq. (2). This table illustrates clearly how  
232 forecasts of the Nile flow can be improved by combining the two indices. For example, “warm”  
233 conditions in both oceans translate into 85% probability of “low” flow in the Nile, and insignificant  
234 probability of “high” flow. On the other hand, “cold” conditions in both oceans translate into 83%  
235 probability of “high” flow in the Nile, and insignificant probability of “low” flow. Depending on  
236 the accuracy of the dynamical forecast models of global SSTs, such forecast of the Nile flow can  
237 be issued with lead times of 6 months. At present, the Eastern Nile Regional technical Office  
238 (ENTRO) issues operational forecasts of the Nile flow based on ENSO forecasts and the  
239 probability table described by Eltahir (1996) (similar to Table 4). We anticipate that use of Table  
240 5, would represent a significant improvement in these operational forecasts.

241 The combined use of ENSO and the SIO indices significantly increased the FI to 0.5 (Figure 8a).  
242 Comparison of Figures 8b and 8c, illustrates that the SIO index alone has almost the same FI value

243 as ENSO index. Recall that in absence of any information about global SSTs, the FI should have  
244 a value of one third. The deviations of the FI using ENSO index alone (Figure 8b) or SIO index  
245 alone (Figure 8c) from one third are almost added together to create the deviation of the FI from  
246 the hybrid method from one third (Figure 8a). Hence, the new SIO index plays an independent role  
247 from ENSO in shaping the interannual variability in the flow of Nile River. Thus by using these  
248 two indices, we explain a significant fraction of the interannual variability in the flow of Nile  
249 River, and illustrate a significant potential for improving the Nile flow forecasts.

## 250 **5. Conclusions**

- 251 • In this paper, we document that the SSTs in the Eastern Pacific and Indian Oceans play a  
252 significant role in shaping the natural interannual variability in the flow of Nile River.  
253 Previous studies have identified a significant teleconnection between the Nile flow and the  
254 Eastern Pacific Ocean. El Niño-Southern Oscillation (ENSO) explains about 25% of the  
255 interannual variability in the Nile flow. Here, this study identifies a region in the southern  
256 Indian Ocean with similarly strong teleconnection to the Nile flow. Sea Surface  
257 Temperature (SST) in the region (50°E-80°E and 25°S-35°S) explains 28% of the  
258 interannual variability in the Nile flow.
- 259 • In addition, four different modes of natural variability in the Nile flow are identified and it  
260 is shown that during non-neutral conditions in both the Pacific and Indian Oceans, the Nile  
261 flow is highly predictable using global SST information. During those years with  
262 anomalous SST conditions in both Oceans, this study estimates that indices of the SSTs in  
263 the Pacific and Indian Oceans can collectively explain up to 84% of the interannual  
264 variability in the flow of Nile. The estimated relationships between the Nile flow and these

265 indices allow for accurately predicting the Nile floods and droughts using observed or  
266 forecasted conditions of the SSTs in the two oceans.

- 267 • This study uses classical Bayesian theorem to develop a new hybrid forecasting algorithm  
268 that predicts the Nile flow based on indices of the SST in the Eastern Pacific and Southern  
269 Indian Oceans. “Warm” conditions in both oceans translate into 85% probability of “low”  
270 flow in the Nile, and insignificant probability of “high” flow. On the other hand, “cold”  
271 conditions in both oceans translate into 83% probability of “high” flow in the Nile, and  
272 insignificant probability of “low” flow. Applications of the proposed hybrid forecast  
273 method should improve predictions of the interannual variability in the Nile flow, adding  
274 a new a tool for better management of the water resources of the Nile basin.

275 The proposed forecasting methodology is indeed dependent on the accuracy of the global SST  
276 forecasts from global dynamical models. The accuracy of these forecasts is likely to improve as  
277 the models are tested and developed further. However, in this paper we test the proposed  
278 forecasting algorithm using observed SSTs. Such test describes an upper limit of the skill of the  
279 proposed algorithm. The assessment of the same methodology using indices of SST forecasted by  
280 global dynamical models will be addressed in future work.

281

282

283

284

285

286

## Tables

287 **Table 1:** Summary of the coefficient of determination ( $R^2$ ) between the average Nile flow from July to  
 288 October and different combination of indices of ENSO and SIO.

Mode		ENSO	SIO	ENSO, SIO	Number of events (Observed Variance of Nile flow)
ENSO	SIO				
Neutral	Neutral	0.04	0.03	0.08	29 (6.76)
Neutral	Non-Neutral	0.05	0.28 <sup>+</sup>	0.31 <sup>+</sup>	26 (10.24)
Non-Neutral	Neutral	0.4 <sup>+</sup>	0.02	0.43 <sup>+</sup>	26 (5.8)
Non-Neutral	Non-Neutral	0.64 <sup>+</sup>	0.6 <sup>+</sup>	0.84 <sup>+</sup>	19 (12.3)

289 SIO: South Indian Ocean SSTs index, ENSO: ENSO index.

290 \*Values that are significant at 5% significance level

291 <sup>+</sup> Values that are significant at 1% significance level

292

293

294

295

296

297

298 **Table 2:** Comparison between regions in the Indian Ocean used in ElDaw et al., 2003 and this  
 299 study to predict the Nile flow.

Region	Location	Study
1	(35°-44° S, 115° -130° E)	ElDaw et al, 2003
2	(0°-7° S, 90° -130° E)	
3	(35°-44° S, 20° -60° E)	
4	(10°-20° S, 110° -125° E)	
5	(50°E-80°E and 25°S-35°S)	This study

300

301 **Table 3:** Conditional probability of the Nile flow given SIO conditions

		Nile flow		
		High	Normal	Low
SIO	Warm	0	0.25	0.75
	Normal	0.23	0.39	0.39
	Cold	0.57	0.26	0.17

302

303

304 **Table 4:** Conditional probability of the Nile flow given ENSO conditions

		Nile flow		
		High	Normal	Low
ENSO	Warm	0.15	0.31	0.54
	Normal	0.22	0.38	0.41
	Cold	0.68	0.32	0

305



306

307 **Table 5:** Conditional probability of the Nile flow given SIO and ENSO conditions

SIO	Nile flow	ENSO		
		Warm	Normal	Cold
SIO Warm	High	0	0	0
	Normal	0.15	0.22	1
	Low	0.85	0.78	0
SIO Normal	High	0.1	0.14	0.57
	Normal	0.31	0.4	0.43
	Low	0.59	0.46	0
SIO Cold	High	0.33	0.42	0.83
	Normal	0.29	0.33	0.17
	Low	0.37	0.25	0

308

309

310

311

312

313

314

315

317 **Table 1:** Summary of some available forecast models of the Sea Surface Temperature

Model	Type of Model	Agency	Domain	Lead time up to (Months)	Resolution (km)	Reference
NCEP-CFS V2	Dynamical	National Centers for Environmental Prediction (NCEP)	Global	8	200	Saha et al., 2010
NASA-GMAO	Dynamical	NASA Goddard Space Flight Center- Global Modeling and Assimilation Office	Global	12	200	Bacmeister et al., 2000
ECMWF-System 4	Dynamical	European Centre for Medium-Range Weather Forecasts	Global	4	70	Molteni et al., 2011
UKMO-GCM	Dynamical	United Kingdom Met Office	Global	6	150	Graham et al., 2005
NOAA-CDC	Statistical	National Oceanic and Atmospheric Administration-Climate Diagnostic Center	Global	12	--	Pneland et al., 1998
CPC-Markov	Statistical	National Centers for Environmental Prediction-Climate Prediction Center	Nino 3 and Nino 3.4	8	--	Xue et al., 2000

319  
320  
321  
322  
323  
324  
325  
326  
327  
328  
329  
330  
331  
332  
333  
334  
335  
336  
337  
338

## REFERENCES

1. Abtew, W., Melesse, A. M. and Dessalegne, T. (2009), El Niño Southern Oscillation link to the Blue Nile River Basin hydrology. *Hydrol. Process.*, 23: 3653–3660. doi: 10.1002/hyp.7367
2. Amarasekera, K. N., Lee, R. F., Williams, E. R., and Eltahir, E. A. B: ENSO and the natural variability in the flow of tropical rivers, *J. Hydrol.*, 200, 24–39, 1996.
3. Beltrando, G., and Camberlin, P., 1993: Interannual variability of rainfall in Eastern Horn of Africa and indicators of atmospheric circulation. *International Journal of climatology* 13, 533-546.
4. Bacmeister, J. T., P. J. Pegion, S. D. Schubert, and M. J. Suarez, 2000: Atlas of seasonal means simulated by the NSIPP1 atmospheric GCM, NASA Tech. Memo-2000-104606, Vol. 17, 194pp.
5. Black E., J. Slingo, and K.R. Sperber, 2003: An observational study of the relationship between excessively strong short rains in coastal East Africa and Indian Ocean SST. *Mon. Wea. Rev.*, 31, 74-94.

- 339 6. Camberlin P., 1995. June-September rainfall in North-Eastern Africa and  
340 atmospheric signals over the tropics: a zonal perspective. *International Journal of*  
341 *Climatology* 15: 773-783.
- 342
- 343 7. Camberlin, Pierre, 1997: Rainfall Anomalies in the Source Region of the Nile and  
344 Their Connection with the Indian Summer Monsoon. *J. Climate*, 10, 1380–1392.
- 345
- 346 8. Conway, D., and M. Hulme, 1993: Recent Fluctuations in precipitation and runoff  
347 over the Nile subbasins and their impact on Main Nile discharge. *Climatic Change*,  
348 25, 127 -151.
- 349
- 350 9. ElDaw, A., J. D. Salas, and L. A. Garcia, 2003: Long Range Forecasting of the Nile  
351 River Flows Using Climate Forcing. *J. Applied Meteorology*, 42:890-904.
- 352
- 353 10. Eltahir, E. A. B., 1996: ElNino and the natural variability in the flow of the Nile  
354 river. *Water Resour. Res.*, 32(1): 131-137.
- 355
- 356 11. Hastenrath, Stefan, Dierk Polzin, and Charles Mutai, 2011: Circulation Mechanisms  
357 of Kenya Rainfall Anomalies. *J. Climate*, 24, 404–412.
- 358 12. Ju, J., and J. M. Slingo, 1995: The Asian summer monsoon and ENSO. *Quart. J. Roy.*  
359 *Meteor. Soc.*, 121, 1133–1168.
- 360

- 361 13. Kawamura, R., 1998: A possible mechanism of the Asian summer monsoon-ENSO  
362 coupling. *J. Meteor. Soc. Japan*, 76, 1009–1027.  
363
- 364 14. Melesse, A., Abtew, W. Setegn, S.G., Desalegn, T. (2011). Hydrological Variability  
365 and Climate of the Upper Blue Nile River Basin. In *Nile River Basin: Hydrology,*  
366 *Climate and Water Use*. Springer. Melesse, Assefa M. (Ed.), 1st Edition., 2011, X,  
367 480 p. 200 illus, Part 1, 3-37, DOI: 10.1007/978-94-007-0689-7\_1  
368
- 369 15. Molteni, F., T. Stockdale, M. Balsaseda, G. Balsamo, R. Buizza, L. Ferranti, L.  
370 Magnusson, K. Mogensen, T. Palmer & F. Vitart, 2011: The new ECMWF seasonal  
371 forecast system (System 4). ECMWF Research Department Technical  
372 Memorandum n.656, ECMWF, Shinfield Park, Reading RG2-9AX, UK, pp. 51.  
373
- 374 16. ElSanabary, M. H., Gan, T. Y., Mwale, D., 204: Application of wavelet empirical  
375 orthogonal function analysis to investigate the nonstationary character of Ethiopian  
376 rainfall and its teleconnection to nonstationary global Sea Surface Temperature  
377 variations for 1900-1998. *International Journal of Climatology*.  
378 DOI:10.1002/joc.3802  
379
- 380 17. Graham. R., M. Gordon, P.J. McLean, S. Ineson, M.R. Huddleston, M.K. Davey, A.  
381 Brookshaw, R.T.H. Barnes, 2005: A performance comparison of coupled and  
382 uncoupled versions of the Met Office seasonal prediction general circulation  
383 model. *Tellus*, 57A, 320-339.  
384

- 385 18. Giro, D. Grimes, D., Black, E. 2011: Teleconnections between Ethiopian summer  
386 rainfall and sea surface temperature: part I Observation and Modeling. *Climate*  
387 *Dynamics* 37:103-199.
- 388  
389 19. Gissila, T., Black, E., Grimes, D. I. F., Slingo, J.M 2004: Seasonal forecasting of the  
390 Ethiopian Summer rains. *International Journal of Climatology* 24: 1345-1358.
- 391
- 392 20. Penland, C. and L. Matrosova, 1998: Prediction of Tropical Atlantic Sea Surface  
393 Temperatures Using Linear Inverse Modeling. *J. Climate*, 11, 483-496.
- 394
- 395 21. Saha, Suranjana, and Coauthors, 2010: The NCEP Climate Forecast System  
396 Reanalysis. *Bull. Amer. Meteor. Soc.*, 91, 1015.1057. doi:  
397 10.1175/2010BAMS3001.1.
- 398
- 399 22. Suranjana Saha, Shrinivas Moorthi, Xingren Wu, Jiande Wang, Sudhir Nadiga,  
400 Patrick Tripp, Hua-Lu Pan, David Behringer, Yu-Tai Hou, Hui-ya Chuang, Mark  
401 Iredell, Michael Ek, Jesse Meng, Rongqian Yang, Huug van den Dool, Qin Zhang,  
402 Wanqiu Wang, Mingyue Chen, 2013 : The NCEP Climate Forecast System  
403 Version 2. (*Journal of Climate*, under review.)
- 404
- 405 23. Shukla, J., and J. M. Wallace, 1983: Numerical simulation of the atmospheric  
406 response to equatorial Pacific sea surface temperature anomalies. *J. Atmos. Sci.*, 40,  
407 1613–1630.

408  
409  
410  
411  
412  
413  
414  
415  
416  
417  
418  
419  
420  
421  
422  
423  
424  
425  
426  
427  
428  
429  
430

24. Siam, M. S., Wang, G., Estelle, ME., and Eltahir, E. A. B, 2014: Role of the Indian Ocean Sea Surface Temperature in shaping natural variability in the flow of the Nile River. *Climate Dynamics*, in press.

25. Soman, M. K., and J. Slingo, 1997: Sensitivity of the Asian summer monsoon to aspects of sea-surface-temperature anomalies in the tropical pacific ocean. *Q. J. R. Meteorol. Soc.*, 123, 309-336.

26. Trenberth, K. E., 1997: The Definition of El Niño. *Bulletin of the American Meteorological Society*, 78, 2771-2777.

27. Wang, G., and Eltahir E. A. B, 1999: Use of ENSO information in Medium and Long Range Forecasting of the Nile Floods . *J. Climate*, 12, 1726-1737.

28. West, M., 1989: *Bayesian Forecasting and Dynamic Models*. Springer, 704 pp.

29. Winkler, R., 1972: *An introduction to Bayesian inference and Decision*. Holt, Rinchart and Winstoon, 563 pp.

30. Xue, Y., A. Leetmaa, and M. Ji, 2000: ENSO prediction with Markov model: The impact of sea level. *J. Climate*, 13, 849-871.

431 31. Yang, J. L., Q. Y. Liu, S. P. Xie, et al., 2007: Impact of the Indian Ocean SST basin  
432 mode on the Asian summer monsoon, *Geophys. Res. Lett.*, 34, L02708,  
433 doi:10.1029/2006GL028571.

434

435

436

437

438

439

440

441

442

443

444

445

446

447

448

449

450

451

452

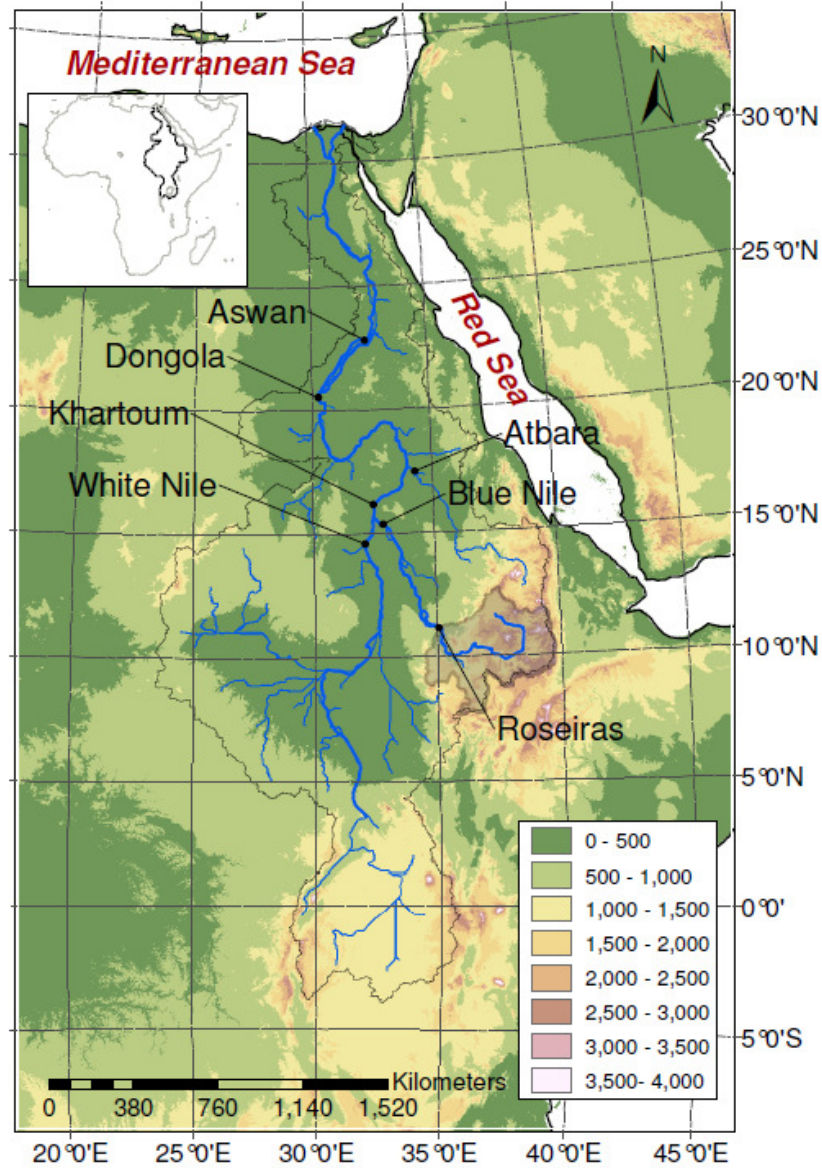
453



# Figures

454

455



456

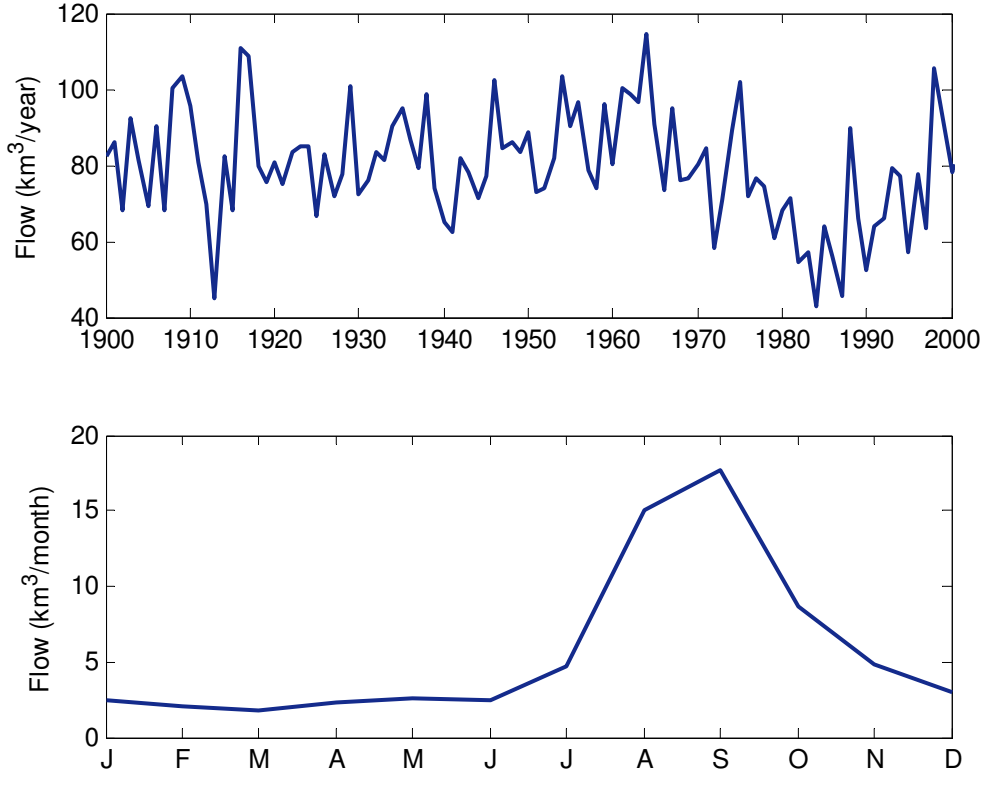
457

458 **Figure 1:** Topographic map of the Nile basin showing the outlet of the Upper Blue Nile basin (shaded in  
459 gray) at Roseiras. The White and Blue Nile join together at Khartoum the form the main branch of the Nile  
460 that flows directly to Dongola in the North.

461

462

463



477 **Figure 2:** Annual Nile flow (Top) and seasonal cycle (Bottom) of the flow at Dongola for the period from  
478 1900 to 2000.

479

480

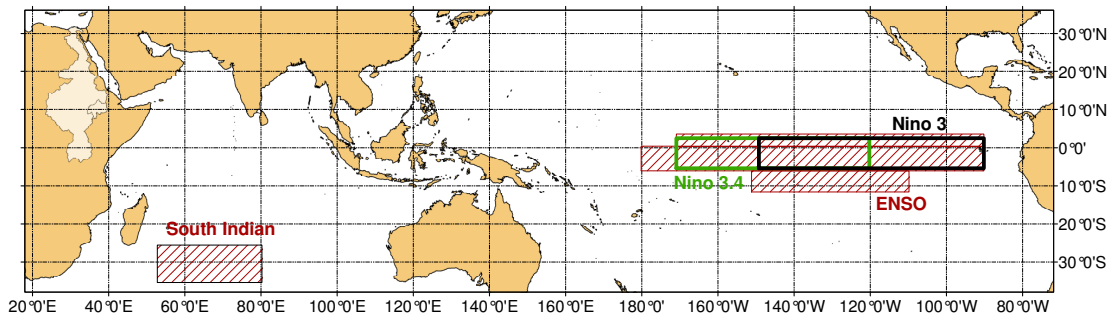
481

482

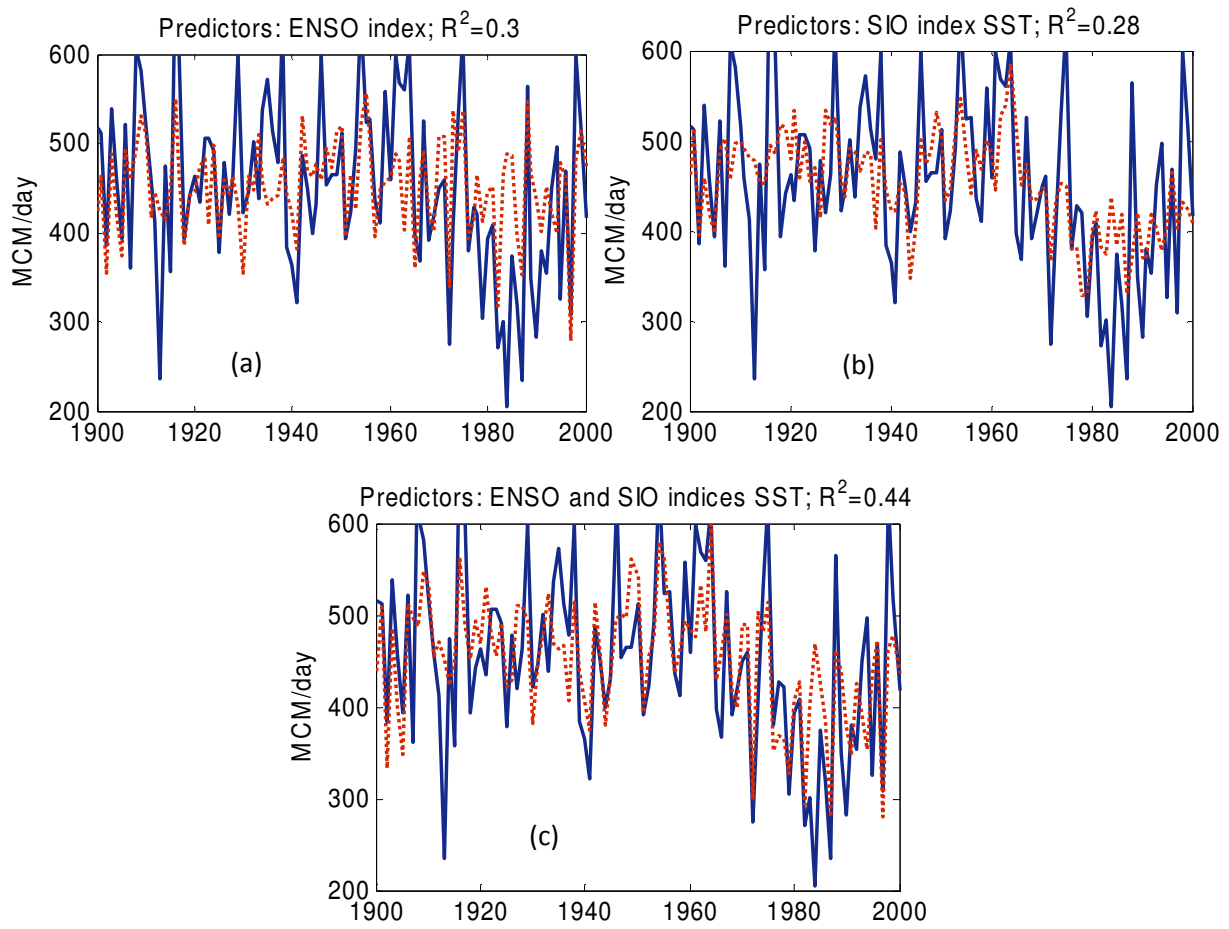
483

484

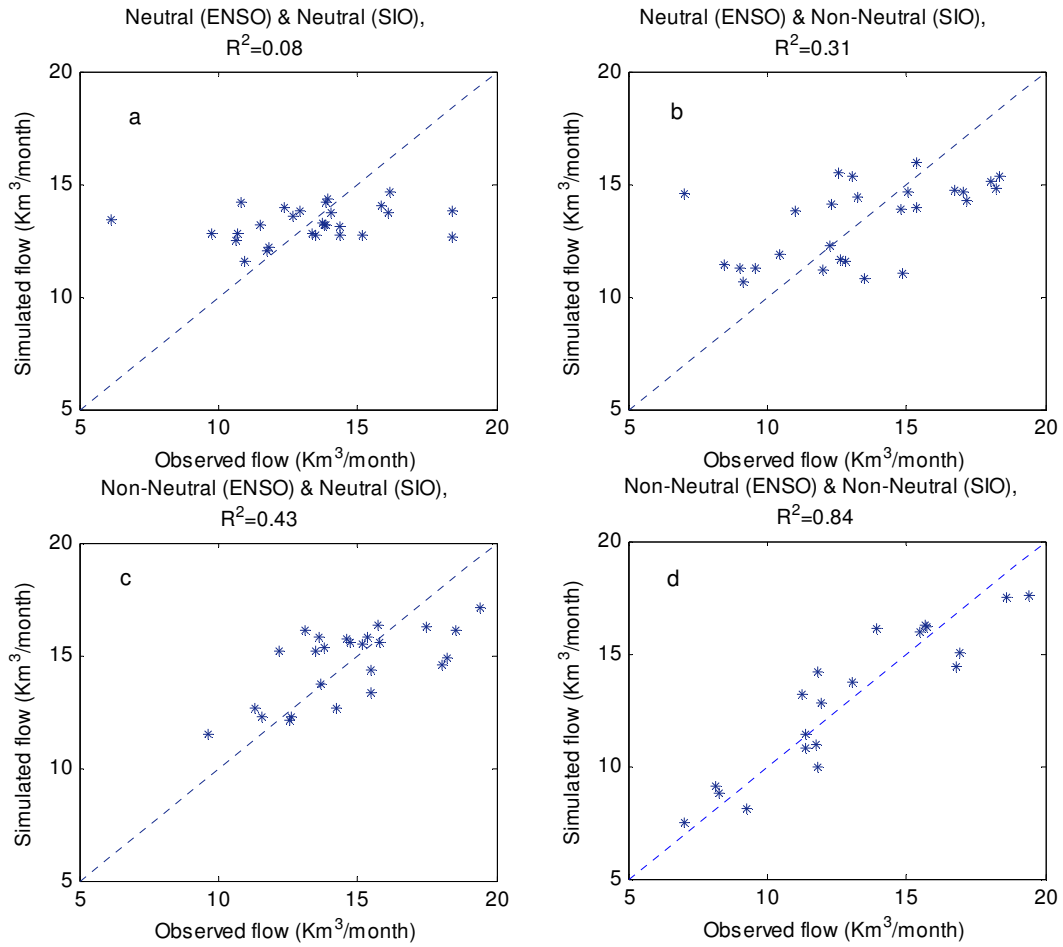
485



486 **Figure 3:** World map showing areas that cover the ENSO and North and South Indian Ocean SSTs indices.  
487 The Nino 3 and 3.4 are outlined in blue and green respectively. The whole Nile basin is outlined in black.



490 **Figure 4:** Observed (Solid Blue lines) and simulated (Dashed Red lines) average Nile flows from July to  
 491 October at Dongola using: a) ENSO index, b) SIO index and c) ENSO and SIO indices as predictors for the  
 492 period 1900 to 2000.



497

498 **Figure 5:** A comparison between the observed and simulated Nile flow showing the different modes of  
 499 variability for the period from 1900 to 2000: a) Neutral ENSO and SIO, b) Neutral ENSO and Non-Neutral  
 500 SSTs in SIO, c) Non-Neutral ENSO and Neutral SSTs in SIO and finally, d) Non-Neutral ENSO and Non-  
 501 Neutral SSTs in SIO.

502

503

504

505

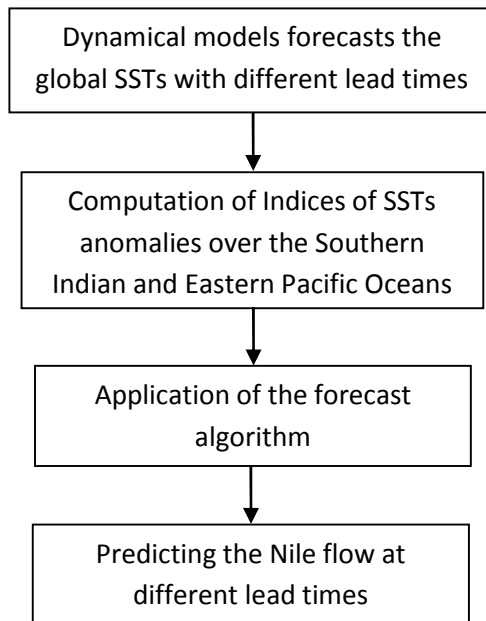
506

507

508

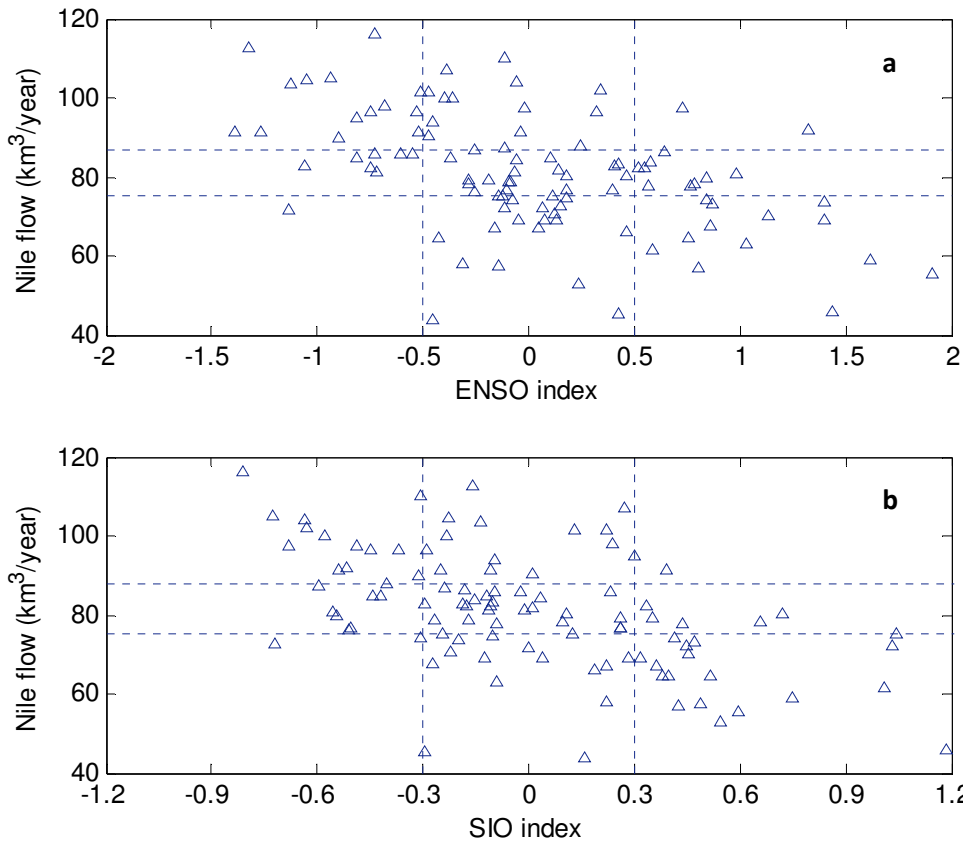
509

510  
511  
512  
513  
514  
515  
516  
517  
518  
519  
520



521 **Figure 6:** Schematic of the hybrid methodology for predicting the Nile flow using the SSTs forecasts of  
522 the dynamical models and the proposed forecast algorithm.

523  
524  
525  
526



527

528 **Figure 7:** Relations between the annual Nile flow and different indices for the period (1900-2000): a)  
 529 ENSO, and b) SIO. The horizontal lines represent the boundaries for the “high”, “normal” and “low”  
 530 categories of the annual flow. The vertical lines represent the boundaries for the “Warm”, “normal”, and  
 531 “cold” conditions for ENSO and SIO indices.

532

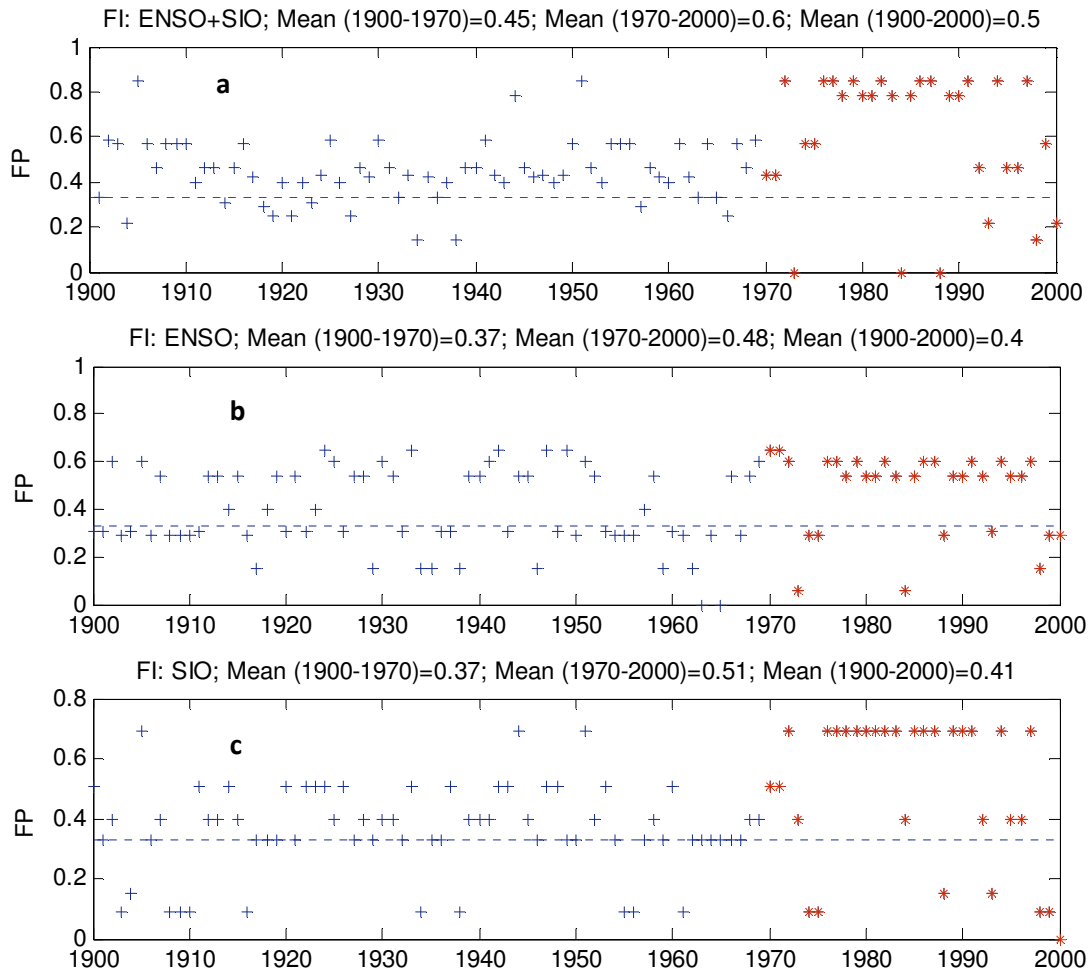
533

534

535

536

537



538

539 **Figure 8:** Time series of the forecast probability using different indices: a) ENSO and SIO together, b)  
 540 ENSO, and c) SIO. The period (1900-1970) is used for calculating the probabilities (shown in crosses)  
 541 using Eq. (2) and (1970-2000) for validation (shown in stars).

542